Hierarchically porous fibrous carbon containing Fe_3O_4 particles and doped with both N and S derived from polypyrrole modified lignosulphonate-bacterial cellulose for use in high performance supercapacitors

Kummara Madhusudana Rao[1,2], Sung Soo Han[1,2,*]

(1. *School of Chemical Engineering*, *Yeungnam University*, 280 *Daehak-Ro*, *Gyeongsan*, *Gyeongbuk*, 38541, *Republic of Korea*;
2. *Research Institute of Cell Culture*, *Yeungnam University*, *Gyeongsan* 38541, *Republic of Korea*)

Abstract: The design of heteroatom-doped porous carbon materials integrated with metal oxide nanostructures has emerged as an efficient approach for improving the electrochemical performance of supercapacitors. A green and cost-effective method is reported for the fabrication of a hierarchical porous carbon composite from bacterial cellulose (BC), lignosulfonic acid (LS), and polypyrrole (PPy). LS serves as both an anchoring agent and a soft molecular template, directing the oxidative polymerization and uniform deposition of PPy onto the BC nanofibers in the presence of $FeCl_3$ as the oxidizing agent. Subsequent carbonization under a nitrogen atmosphere results in the formation of an N/S co-doped carbon framework decorated with Fe_3O_4 nanoparticles, which is denoted C-BCLP. For comparison, a control composite consisting of BC and PPy without LS was carbonized to produce C-BCP. X-ray diffraction patterns confirms the synthesis of Fe_3O_4 nanoparticles and the preservation of the fibrous carbon structure. Electron microscopy shows that C-BCLP has a highly porous and conductive network with a homogeneous distribution of C, O, N, S and Fe elements. Because of the combined effects of hierarchical porosity, heteroatom doping, and Fe_3O_4 incorporation, the C-BCLP electrode has high specific capacitances of 338.3 F g^{-1} at 1 A g^{-1} and 191.6 F g^{-1} at 10 A g^{-1}. In addition, it has excellent cycling stability, retaining 99.1% of its initial capacitance after 10 000 charge-discharge cycles, outperforming the C-BCP electrode. The work suggests a promising way to develop next-generation high-performance supercapacitors.

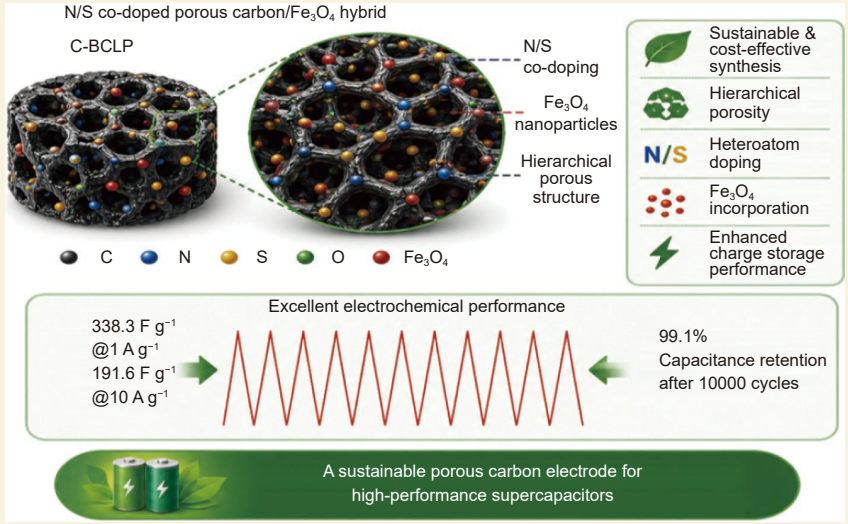

Key words: Bacterial cellulose; Hetero atom doping; Fe_3O_4; Porous carbon; Supercapacitor

1 Introduction

The need for sustainable and efficient energy storage devices has led to an extensive study of advanced electrode materials for supercapacitors. Supercapacitors are promising devices for efficient energy storage due to their rapid charge-discharge rates, high power density, and long cycle life[1–2]. However, the low energy density of supercapacitors remains a significant drawback, which can be controlled by the electrochemical properties of the electrode materials[3–4]. Therefore, it is important to design new electrode materials with high electrical conductivity, large surface area, and electroactivity to enhance the effi-

Received: April 05, 2026
Revised: June 01, 2026
Accepted: June 02, 2026

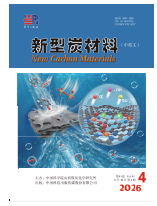

ciency of supercapacitors.

Carbon nanomaterials such as activated carbon materials, graphene, and carbon nanotubes have been extensively used for supercapacitors due to their high electrical conductivity and chemical stability[5–7]. However, these materials have complex synthetic routes and use nonrenewable sources, posing environmental and economic issues. Recent studies have shown that biomass-derived carbon materials have great potential for use in supercapacitors because of their renewability, porosity, and possibility of introducing heteroatoms during the carbonization process[8–9]. These properties allow for the production of hierarchical porous carbon materials that can enhance the efficiency of the electrolyte penetration and ion transport.

Among various biomass sources, bacterial cellulose (BC) has shown great potential for use in supercapacitors because of its 3D nanofibrous structure, high purity, and mechanical strength[10]. After the carbonization of BC, a hierarchical structure of carbonized BC (C-BC) can be formed, which has good electrical conductivity and porosity. The structure of C-BC has great potential for use in supercapacitors because of its hierarchical structure, which can allow efficient penetration of the electrolyte[11–13]. Although C-BC has good porosity and structure, it has low electrical conductivity and electroactivity, limiting its use for supercapacitors[10, 14]. To further improve the electrochemical performance of C-BC materials, various heteroatom doping strategies have been investigated[15–18]. The incorporation of heteroatoms such as nitrogen and sulfur into carbon materials has shown great potential in enhancing the electrochemical performance by changing the electronic structure and increasing the surface polarity[17–18]. As mentioned earlier, sodium lignosulphonate (LS) is used as the sulfur source and is doped into the BC matrix before carbonization to produce sulfur-doped carbon materials (C-BCL)[19]. The C-BCL materials exhibited improved electrochemical performance compared with the pristine C-BC materials. Nevertheless, further enhancement of the electrical conductivity and electrochemical activity remains necessary to fully exploit their energy-storage potential and achieve superior electrochemical performance.

In recent studies, researchers have proposed an effective way to further enhance the electrochemical performance of biomass-derived carbon materials by introducing heteroatoms and conductive polymer modification[20]. Conductive polymers such as polypyrrole (PPy) have shown excellent electrical conductivity and redox activity and are used as nitrogen sources to produce nitrogen-doped carbon materials during carbonization[21]. The incorporation of nitrogen and sulfur heteroatoms into the carbon materials produce synergistic effects and further enhance their electrochemical performance[22]. Furthermore, the integration of transition metal oxides into conductive carbon matrices was also observed to increase the pseudocapacitive properties[23]. Among the various transition metal oxides considered for pseudocapacitive applications, magnetite (Fe_3O_4) was found to be a promising material due to its various oxidation states, low cost, environmental sustainability, and high theoretical capacitance[24]. When integrated into conductive carbon matrices, Fe_3O_4 nanoparticles were observed to provide additional redox reactions while maintaining structural stability[25–27]. Despite the various developments in the pseudocapacitive properties of carbon materials, the exploration of BC-derived carbon materials that can effectively integrate polymer-assisted heteroatom co-doping and metal oxide pseudocapacitance is still in its early stages. In this regard, the influence of polymer structural engineering on the electrochemical properties of C-BC materials is still to be investigated.

In this study, we propose a sustainable route to nitrogen/sulfur co-enriched carbon/Fe_3O_4 hybrid electrodes (C-BCLP) based on a precursor of PPy-modified LS impregnated on BC. The hybrid materials, in which LS is used as a sulfur source and PPy as a nitrogen-rich conductive polymer, show superior electrochemical activity. The hierarchical porosity of these materials is favorable for electroactive sites. The addition of Fe_3O_4 to the hybrid systems increases the electrical conductivity and aids in electron transport in the

heteroatom-doped porous carbon system. The electrochemical performance of the hybrid materials surpasses that of previously reported carbon materials derived from BC and BC-LS precursors. This enhanced performance can be attributed to the synergistic effects of hierarchical porosity, heteroatom doping, and improved electrical conductivity arising from the incorporation of Fe_3O_4 nanoparticles. The physical and electrochemical properties of such materials were thoroughly examined for use in high-performance supercapacitors.

2 Materials and methods

2.1 Materials

BC sheets were collected by culturing Gluconacetobacter hansenii PJK (G. hansenii PJK) bacteria, supplied from the American Type Culture Collection (ATCC 8246) and the National Collections of Industrial and Marine Bacteria (NCIB). The bacterial cellulose was produced using the method that was previously published. LS, pyrrole (Py) monomer, ferric chloride ($FeCl_3$), and other chemicals were obtained from Sigma-Aldrich.

2.2 Preparation of C-BCP and C-BCLP

For the synthesis of the LS-functionalized sample, BC films were soaked in a LS aqueous solution (1 mg mL^{-1}) and stirred for 12 h to enable the LS adsorption onto the BC films. After adsorption, 50 mL of Py monomer (Py) solution (0.1 mol L^{-1}) was added to the BC-LS mixture and stirred to ensure uniform dispersion. Oxidative polymerization of Py was initiated by the gradual addition of 50 mL of $FeCl_3$ solution (0.2 mol L^{-1}), which served as the oxidizing agent. The reaction mixture was continuously stirred for 6 h to enable homogeneous polymerization and composite formation. The resulting composite was thoroughly washed with deionized water and ethanol to remove residual reactants and impurities, followed by freeze-drying. The dried composite was then carbonized at 800 °C for 2 h under nitrogen atmosphere, yielding an N/S co-doped carbon material embedded with Fe_3O_4 nanoparticles, denoted as C-BCLP. For comparison, a control sample was prepared following the same procedure in the absence of LS. The resulting carbonized BC/PPy composite was designated as C-BCP.

2.3 Characterization

The crystal structures of the synthesized electrode materials, namely, C-BCP and C-BCLP, were characterized using X-Ray Diffraction (XRD) analysis on a Bruker D8 Advance X-Ray Diffractometer equipped with Cu *K*α radiation (λ = 1.54 Å) to study the phase composition and structural properties of the materials after carbonization. The surface morphology and microstructures of the synthesized composites were characterized using Field Emission Scanning Electron Microscopy (FE-SEM) (JEOL JSM-7600F), which revealed detailed information about the fibrous architecture of the carbon materials. Additionally, the internal structures and nanomorphologies of the synthesized composites, namely, C-BCP and C-BCLP, were characterized using Transmission Electron Microscopy (TEM) (JEOL JEM-2100), which revealed the fibrous architecture of the carbon materials and the distribution of Fe_3O_4 nanoparticles within the carbon structures. The elemental composition and chemical states of the elements in the composites were characterized using X-Ray Photoelectron Spectroscopy (XPS) (Thermo Scientific K-Alpha XPS system), which revealed the presence of heteroatom doping of nitrogen and sulfur and the oxidation states of iron in the carbon structures. The above-mentioned characterizations of the synthesized composites, namely, C-BCP and C-BCLP, have been carried out in detail for the potential application of the materials as electrode materials in supercapacitor devices.

2.4 Electrochemical test

The electrochemical properties of the synthesized C-BCP and C-BCLP electrodes were examined using a three-electrode system with a potentiostat/galvanostat. Commercially available Ni foam with a thickness of 1.6 mm (MTI Corporation) was utilized for the electrode preparation. Prior to electrode fabrication, the Ni foam was cleaned by sequential ultrasonication in 1 mol L^{-1} HCl solution, deionized (DI) wa-

ter, and absolute ethanol for 10 min each to remove surface impurities and contaminants. For the electrode preparation, the Ni foam with dimensions of 2.5 cm × 1 cm was utilized as the substrate. The homogeneous mixture of the active materials, i.e., C-BCP or C-BCLP, polyvinylidene fluoride (PVDF) as the binder, and carbon black as the conductive material in the ratio of 8∶1∶1 were dispersed in 0.6 mL of NMP solution. The obtained homogeneous mixture was then dropped over the Ni foam substrate with dimensions of 1 cm × 1 cm and dried at 80 °C for 9 h. The average mass loading of the active material on the electrodes was approximately 2 mg. The electrochemical tests, including cyclic voltammetry (CV), galvanostatic charge/discharge (GCD), and electrochemical impedance spectroscopy (EIS), were performed using a Bio-Logic SP-200 Potentiostat/Galvanostat from Bio-Logic Science Instruments. These tests were performed for the purpose of investigating the capacitive behavior of the C-BCP and C-BCLP electrode materials for supercapacitor devices. The value of the specific capacitance (C_s), which is an important factor of performance, was determined by the Eq. (1)

$$C_s = (I \times \Delta t)/(\Delta V \times m) \quad (1)$$

where C_s (F/g) based on potential window from −1.0 to 0 V. Several important factors were considered in the equation including current density (I), discharge time (Δt), potential window (ΔV), and weight of active material (m).

3 Results and discussion

3.1 Production of C-BCLP composite

Scheme 1 represents the formation of C-BCLP nanocomposite. Purified BC nanofibers were first impregnated with a solution of pyrrole monomer, followed by in situ oxidative polymerization of the monomer by $FeCl_3$, yielding a BC/PPy composite, in which uniform coatings of PPy were formed on the BC nanofibers[28]. For the LS-modified counterpart, BC nanofibers were first impregnated with a solution of LS and then reacted with a solution of Py monomer in the presence of $FeCl_3$, yielding a BC/LS/PPy composite. The as-prepared precursors were then freeze-dried to retain their nanofibrous structure, followed by carbonization at 800 °C in nitrogen atmosphere for 2 h, during which significant structural changes occurred. Specifically, in the course of carbonization, the nanofibrous structure of BC nanofibers was retained as a structural template, converting into a conductive carbon structure. At the same time, PPy was thermally decomposed into N-doped carbon materials, in which nitrogen has different bonding states pyrrolic, and graphitic nitrogen can improve electrical conductivity. For the BC/LS/PPy counterpart, in the course of thermal treatment, LS was thermally decomposed, introducing sulfur heteroatoms into the carbon structure, as well as creating structural defects[19], which can improve surface reactivity and adsorption of ions in an electrolyte solution. Meanwhile, $FeCl_3$ not only acted as an oxidizing agent for the polymerization of Py but was also utilized as a metal source for the synthesis of Fe_3O_4 nanoparticles from Fe^{3+} ions, which were carbonized into the carbon framework[29, 30]. As such, the final product was C-BCP, an N-doped porous carbon derived from BC-PPy, whereas the other product, C-BCLP, was derived from BC-LS-PPy and consisted of hierarchically porous N/S co-doped carbon-Fe_3O_4 composite. The combination of the carbon framework derived from BC, het-

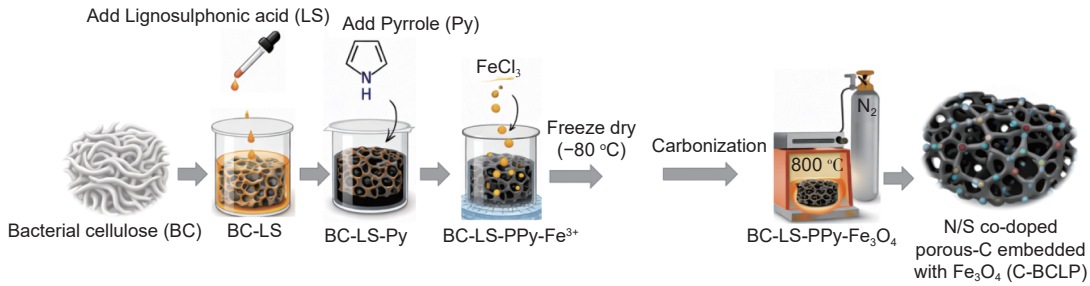

Scheme 1 Schematic illustration of the formation process of C-BCLP

eroatom doping, and Fe_3O_4 nanoparticles is expected to enhance electron transport, provide additional Faradaic redox reactions, and allow for rapid ion transport. As such, the electrochemical performance of the synthesized C-BCP and C-BCLP materials was examined for their application in supercapacitor electrodes.

3.2 XRD patterns

Initially, the formation of Fe_3O_4 and the crystalline nature and phase of carbonized composite were identified using XRD (Fig. 1). As observed from the diffraction pattern, a broad and disordered diffraction peak is observed at $2\theta \approx 24°–26°$, corresponding to the (002) plane of graphitic carbon[19]. This broad diffraction peak is indicative of an amorphous/turbostratic carbon phase formed due to carbonization of PPy and LS in BC. The low intensity and broad nature of this diffraction peak suggest partial graphitization with defects, which are advantageous for improving accessibility of ions and providing electrochemically active sites. Apart from the carbon feature, several sharp diffraction peaks can be observed at $2\theta \approx 30.2°$, 35.5°, 43.2°, 57.1° and 62.8°. These diffraction peaks can be indexed to the (220), (311), (400), (511) and (440) crystal planes of cubic Fe_3O_4, respectively (JCPDS card No. 19-0629)[30]. The absence of impurity peaks in the diffraction spectrum confirms the successful in situ formation of pure Fe_3O_4 during thermal treatment. The sharpness and high intensities of the diffraction peaks indicate that Fe_3O_4 nanoparticles have good crystallinity. This confirms that the coordination of Fe^{3+} ions during oxidative polymerization effectively regulates the formation of Fe_3O_4 nanocrystals during carbonization. Notably, the co-existence of amorphous carbon and Fe_3O_4 nanocrystals in the diffraction spectrum confirms that a well-integrated hybrid structure has been formed. The carbon matrix not only maintains the fibrous structure of BC but also acts as a conductive medium for efficient electron transfer. The Fe_3O_4 nanocrystals contribute to additional improvement in the conductivity. The structural configuration of the hybrid composite, as confirmed by the XRD patterns, accounts for the excellent electrochemical performance of the composite electrode.

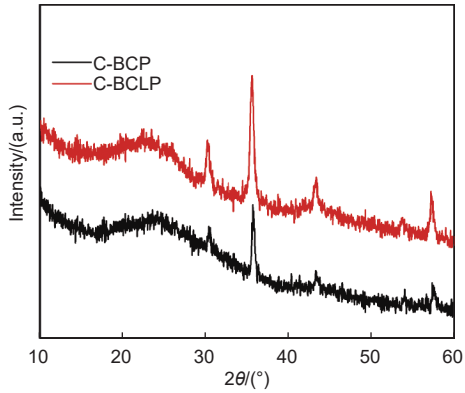

Fig. 1 XRD patterns of C-BCP and C-BCLP

3.3 Morphological study

The morphological evolution and elemental distribution of the composite materials were analyzed using SEM and EDS mapping (Fig. 2). As illustrated in Fig. 2a, it is evident that the composite maintains its inherent 3D interconnected nanofibrous structure of BC signifying that the oxidative polymerization of Py did not compromise the structural integrity of the biomass host material. Instead, PPy uniformly coats the cellulose nanofibers, creating a rough surface texture. Element mappings (a-2 to a-5) of the composite indicate a homogeneous distribution of carbon and oxygen from the cellulose backbone and nitrogen from PPy, signifying the successful synthesis of PPy. Additionally, iron is present in the mapping, signifying coordination with iron ions during the oxidative polymerization of pyrrole using $FeCl_3$, which is essential for metal oxide formation[28].

After incorporating LS and carbonization, the surface of the C-BCLP (BC-LS-PPy-Fe_3O_4) composite (Fig. 2b) is more textured and granular, with nanoparticles dispersed throughout the carbonized fibrous network. Significantly, the fibrous morphology is very well maintained, indicating that the precursor material is effective in stabilizing the framework even under high-temperature conditions. Elemental mappings b-2 to b-6 show a carbon network with uniformly dispersed nitrogen and sulfur species, indicating successful nitrogen and sulfur co-doping from PPy and LS, respectively. Uniform iron distribution confirms that

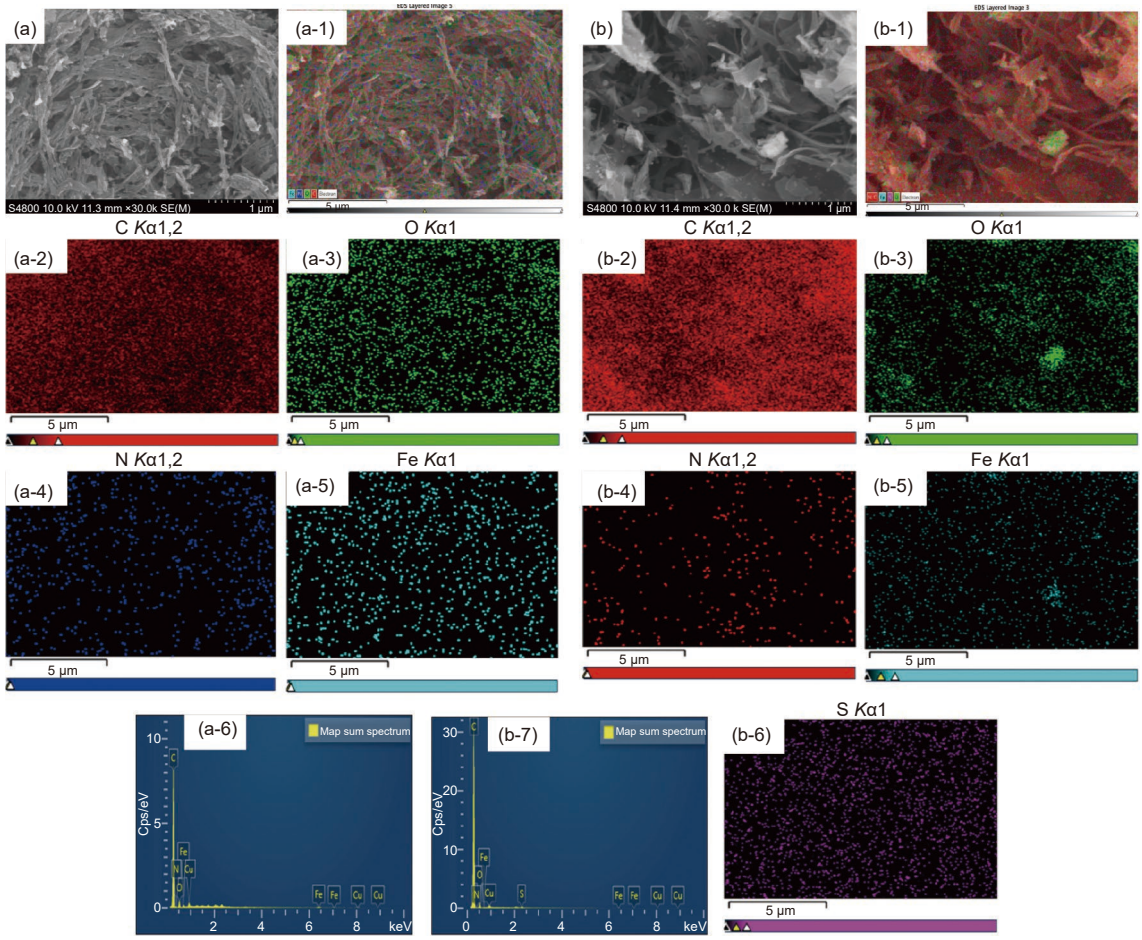

Fig. 2　SEM images of (a, a-1) C-BCP and (b, b-1) C-BCLP showing the fibrous porous carbon structure. (a-2 – a-5) EDS elemental mapping of C, O, N, and Fe for C-BCP, (a-6) EDX spectrum for the confirmation of the elements. (b-2 – b-5) EDS mapping of C, O, N, and Fe for C-BCLP, (b-6) S elemental mapping, and (b-7) EDX spectrum for the confirmation of the elements

iron is uniformly dispersed throughout the carbon network without any signs of agglomeration, indicating the formation of uniformly dispersed Fe_3O_4 nanoparticles. EDS spectra of these mappings clearly show the presence of C, O, N, S and Fe, indicating successful construction of a carbon-metal oxide hybrid with multiple heteroatoms. This homogeneous heteroatom incorporation and nanoscale dispersion of Fe_3O_4 confirm the critical role of the polymer-modified LS-BC precursor in controlling interfacial coordination and nucleation during carbonization. This integrated architecture should allow for enhanced electrical conductivity, site density of redox functionalities, and ion diffusion through the porous material. Thus, the observed morphology and elemental composition confirm the structural basis of the enhanced electrochemical performance of the composite, where electric double-layer capacitance from the conductive carbon phase is expected to complement pseudocapacitive contributions from the N/S functionalities and Fe_3O_4 redox sites.

The microstructure of the synthesized C-BCLP composite was characterized by TEM to observe the internal structure of the composite. From the TEM images in Fig. 3(a & a-1), it is apparent that the composite has a porous structure consisting of a fibrous carbon structure resulting from the BC. This porous structure is advantageous because it can conduct electrical current while allowing the penetration of an electrolyte[31]. From the high-magnification TEM image in Fig. 3(a-2), it is apparent that the composite has dark contrast nanoparticles. This indicates that the composite has Fe_3O_4 particles resulting from the thermal conversion of Fe^{3+}. Obviously, the in situ polymerization reaction that occurred in the composite was effective because it prevented aggregation of

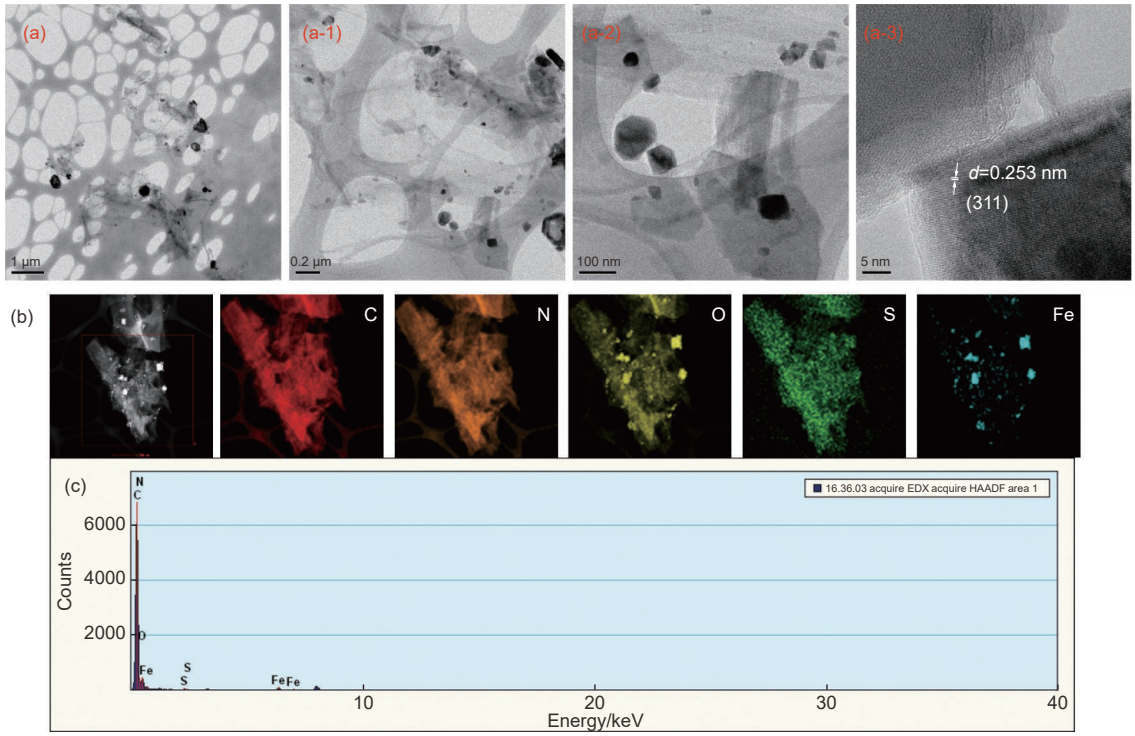

Fig. 3 TEM analysis of C-BCLP. (a−a-3) TEM images at different magnifications of the porous carbon structure obtained from bacterial cellulose with dispersed nanoparticles.(b) Elemental mapping images showing the uniform distribution of C, N, O, S and Fe elements in the carbon structure. (c) EDX spectrum showing the presence of C, N, O, S and Fe elements in the C-BCLP composite material

the particles.

The well-defined structure of carbon observed from the high-resolution TEM image in Fig. 3(a-3) suggests that there are partially graphitized structures in the C-BCLP composite, which would help in improving electrical conductivity and facilitating faster charge transfer during electrochemical reactions. The elemental composition and distribution in the composite material have also been studied further with TEM-EDS elemental mapping, which confirmed the uniform distribution of C, N, O, S and Fe in the C-BCLP composite material. The nitrogen present in the composite is from the carbonization of PPy, while sulfur is introduced from LS during the thermal treatment. Iron is present in the form of Fe_3O_4 nanoparticles. In addition to this, the EDX spectrum shown in Fig. 3c quantitatively confirms the elemental composition present in the RGC composite material. The percentages obtained from the EDX analysis are: C: 92.93%, N: 3.00%, O: 2.98%, S: 0.21%, and Fe: 0.86%, respectively. The elemental composition obtained from the EDX analysis is consistent with the elemental composition obtained from the SEM-EDS mapping and the surface chemical analysis obtained from X-ray Photoelectron Spectroscopy (XPS) studies. Furthermore, the experimentally observed lattice fringes corresponding to an inter-planar distance of 0.253 nm relate to the (311) plane of the crystal structure of Fe_3O_4, thus indicating that Fe_3O_4 nanoparticles have been formed successfully (Fig. 3 (a-3)). Therefore, it is evident that, as concluded in the TEM images, the C-BCLP composite is composed of a hierarchical porous carbon structure with uniformly dispersed heteroatoms and Fe-based nanoparticles, forming an N/S co-doped C-Fe_3O_4 hybrid material. The structural features of this material could improve its electrochemical activity for high-performance supercapacitor electrode applications.

3.4 XPS spectra

XPS analysis was carried out to investigate the surface chemistry of the formed C-BCLP composite. High-resolution spectra of the C 1s, N 1s, Fe 2p and S 2p levels are shown in Fig. 4a. The survey spectrum shows the presence of C, N, O, S and Fe. From the

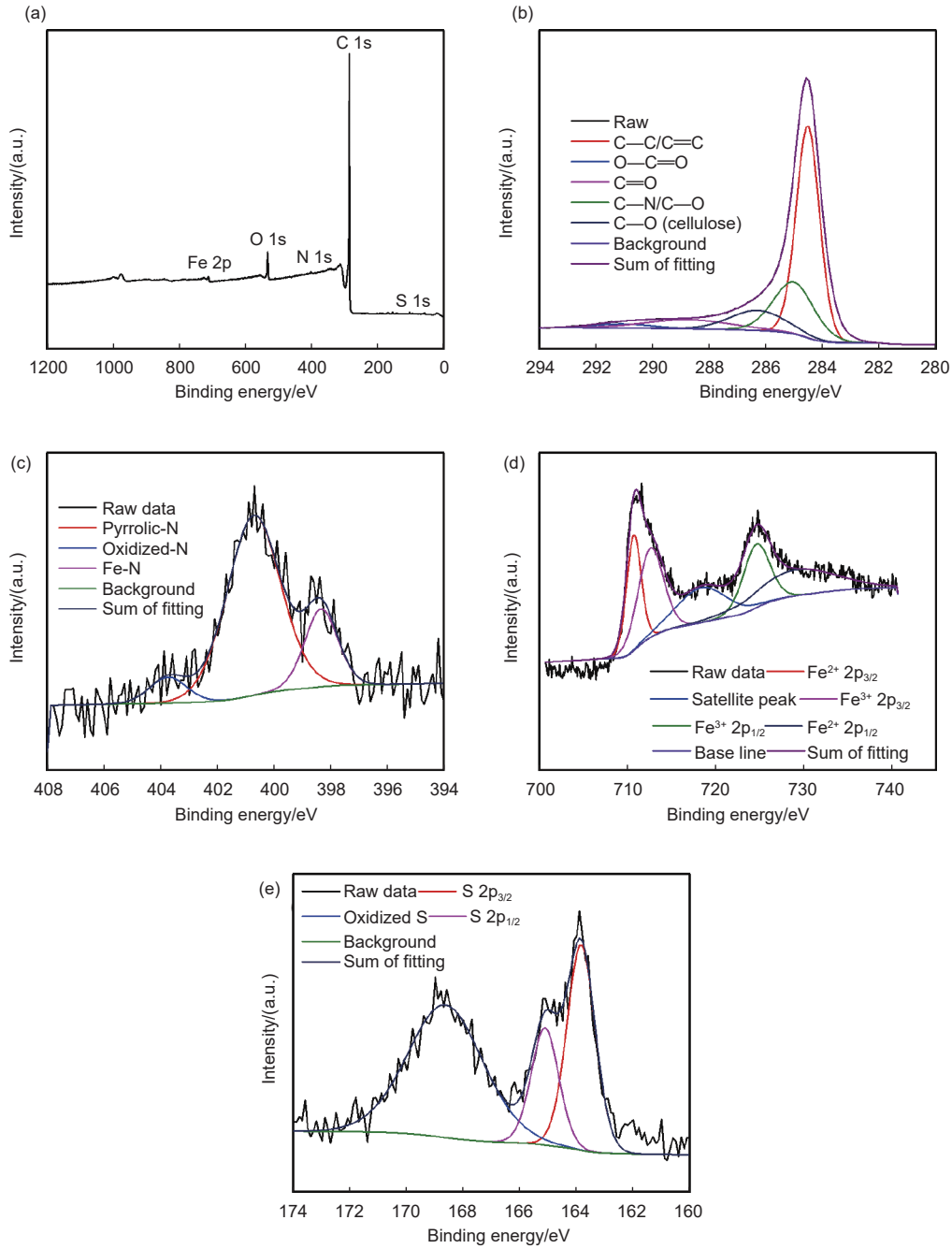

Fig. 4　(a) Survey XPS spectrum and high-resolution XPS spectra of (b) C 1s, (c) N 1s, (d) Fe 2p and (e) S 2p binding energies of C-BCLP composite

results obtained from the analysis of the XPS survey, it is evident that the C, O, N, S and Fe elements were successfully incorporated in the synthesized C-BCLP material. In the XPS survey scan, the predominant peak observed with C 1s at 284.56 eV has an atomic percent of 91.65%, which suggests that the prepared material contains a high content of the carbon framework that leads to the electric double-layer capacitance properties as well as enhanced electrical conductivity. The O 1s peak at 532.38 eV has an atomic percent of 6.38%, indicating the presence of O atoms in the material structure due to oxygen-containing functional groups and surface adsorption. The N 1s peak at 400.7 eV proves successful doping with nitrogen into the carbon framework. On the other hand, the S 2p peak at 163.9 eV shows successful doping of sulfur into the carbon structure. Successful doping of N and S heteroatoms enhances the surface wettability as well as improves charge transfer characteristics. Besides, the Fe 2p peak at 711.12 eV clearly demon-

strates the presence of Fe_3O_4 nanoparticles incorporated into the carbon matrix. Though the Fe atoms are present in trace amounts (0.71%), the Fe_3O_4 nanoparticles help in improving electrical conductivity. This is consistent with the elemental composition observed using SEM-EDS and TEM-EDS. This confirms the integration of the heteroatoms and iron oxide. The high-resolution C 1s spectrum in Fig. 4b can be deconvoluted to several peaks that correspond to different C bonding environments. The dominant peak at ~ 284.6 eV is associated with sp^2-hybridized C—C/C=C bonds in the graphitic network created by the carbonization of bacterial cellulose and polypyrrole. The secondary peak at ~ 285.6 eV is associated with C—N/C—O bonds that arise from nitrogen content in the carbon matrix from the carbonization of polypyrrole and from oxygen in the cellulose. The third peak at ~ 286.7-287.2 eV is associated with C=O bonds, while the high-binding energy peak at ~ 288.5 eV is associated with O—C=O bonds. The C=O and O—C=O bonds can be associated with LS and oxidized carbon. The presence of these oxygen- and nitrogen-based functional groups can contribute to an increased surface polarity and wettability of the electrolyte. The N 1s XPS spectrum (Fig. 4c) shows the successful incorporation of nitrogen species in the carbon matrix. The major source is the carbonization of PPy. The deconvoluted peaks correspond to Fe—N bonding (~ 398.7-399.0 eV), pyrrolic-N (~ 400.1 eV), and a small peak for oxidized-N (~ 402-403 eV). Pyrrolic-N is known to contribute to pseudocapacitance due to the electrochemically active sites for reversible redox reactions. The presence of Fe-N bonding indicates the potential for coordination interactions between the nitrogen species and iron. This could result in an improvement in electrical conductivity. The small peak for oxidized-N could be due to the presence of oxygen in the biomass precursor. The Fe 2p high-resolution spectrum (Fig. 4d) also verifies that iron oxide species are present in the carbon matrix. The binding energies of ~ 710.8 and ~ 724.5 eV are related to Fe^{2+} $2p_{3/2}$ and Fe^{2+} $2p_{1/2}$, whereas ~ 712.5 and ~ 726.1 eV are related to Fe^{3+} $2p_{3/2}$ and Fe^{3+} $2p_{1/2}$, respectively. In addition, a satellite peak observed at ~ 719 eV is also related to the coexistence of Fe^{2+} and Fe^{3+} species, which is a characteristic of Fe_3O_4 (magnetite). These observations are also verified by the XRD patterns, where Fe_3O_4 crystalline phases are formed. The presence of Fe^{2+} and Fe^{3+} species verifies that Fe_3O_4 nanoparticles are formed during the carbonization process. The S 2p spectrum (Fig. 4e) again confirms the incorporation of sulfur species derived from LS. The peaks at ~ 163.8 eV for S $2p_{3/2}$ and ~ 165.0 eV for S $2p_{1/2}$ are characteristic of thiophene-like sulfur species, thus proving successful sulfur doping into the carbon lattice[19]. Another peak in the range of ~ 168-170 eV corresponds to oxidized sulfur species, $–SO_x$, which may arise from partial oxidation or thermal decomposition of LS during carbonization. The incorporation of sulfur into the carbon lattice may result in structural defects, thus enhancing electrical as well as electrochemical properties. It can be seen that the results are in good agreement with those from structural and morphological analysis carried out using XRD, SEM and TEM techniques. The Fe^{2+}/Fe^{3+} peak indicates the successful synthesis of Fe_3O_4 nanoparticles, as evidenced in TEM images as dark contrast particles and in XRD patterns as characteristic peaks for Fe_3O_4 nanoparticles. In addition, the detection of nitrogen and sulfur species indicates successful heteroatom doping with species derived from PPy and LS, respectively, as evidenced in elemental mapping carried out using SEM-EDS and TEM-EDS. It is obvious that graphitic carbon, heteroatom doping, and Fe_3O_4 nanoparticles are present in a hierarchically structured composite, which is expected to have good electrical conductivity, a high number of electroactive sites, and good ion transport properties. From the XPS results, it is clearly shown that a hetero atom doped carbon-Fe_3O_4 hybrid material has been successfully synthesized. The dopants of nitrogen and sulfur modify the electronic structure of the carbon framework, whereas the Fe_3O_4 nanoparticles contribute additional faradaic redox reactions. The effect of the constituents is expected to enhance the electrochemical properties of the C-BCLP

electrode for high-performance supercapacitors.

3.5 Electrochemical study

The electrochemical properties of the prepared electrodes of C-BCP and C-BCLP materials have been investigated using CV, GCD, and EIS techniques in a three-electrode system with 3 mol L^{-1} KOH aqueous solution (Fig. 5). The electrochemical properties of the prepared electrodes have been compared with the electrochemical properties of the previously reported carbonized bacterial cellulose (C-BC) and S-carbon materials prepared from LS-impregnated BC.

The CV curves for the C-BCP and C-BCLP electrodes recorded for various scan rates from 5 to 200 mV s^{-1} display a quasi-rectangular shape with the presence of redox peaks (Fig. 5a&b). This indicates the presence of a hybrid electrochemical storage mechanism involving electric double-layer capacitance (EDLC) and pseudocapacitance. The other noticeable point is that the CV curves of the C-BCLP electrode reveal a significantly greater area than that of the C-BCP electrode at all scan rates. This reveals that the electrochemical energy storage of the C-BCLP electrode is superior to that of the C-BCP electrode. The retention of the shape of the CV curve at a higher scan rate implies that the process of ion diffusion and electron transport inside the carbon skeleton of hierarchical porosity occurs rapidly. In comparison to our earlier-reported BC-based carbon and S-doped carbon electrodes, the current electrode demonstrates improved electrochemical behavior while retaining mostly EDLC behavior owing to the predominance of the porous carbon structure. The increased electrical conductivity and electrochemical activity of the electrode can be attributed to the presence of the N/S heteroatoms and uniform distribution of Fe_3O_4 nanoparticles inside the carbon matrix[32, 33].

The results obtained from the GCD measurements again proved the excellent capacitive performance of the C-BCLP electrode (Fig. 5d). The charge-

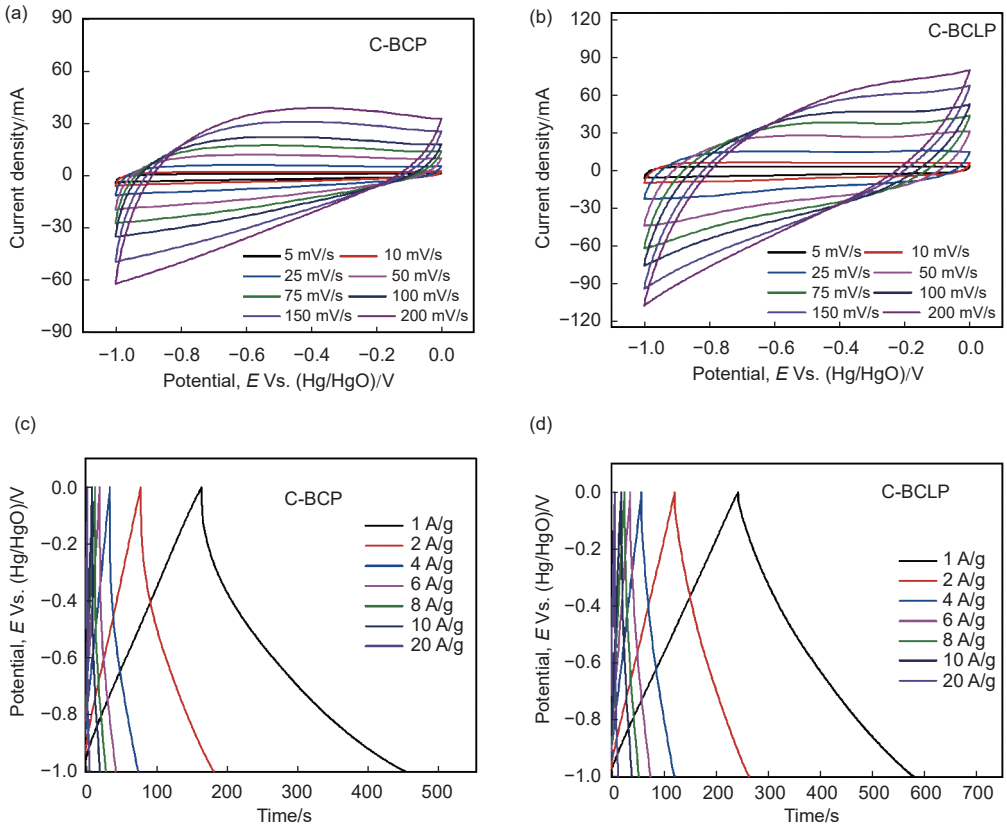

Fig. 5 Representative electrochemical performance of the (a) C-BCP and (b) C-BCLP electrodes in 3 mol L^{-1} KOH electrolyte: (a, b) cyclic voltammograms recorded at various scan rates from 5 to 200 mV s^{-1} within the potential window of −1.0 to 0 V versus Hg/HgO, and (c, d) galvanostatic charge-discharge curves measured at different current densities from 1 to 20 A g^{-1}

discharge curves show quasi-triangular shapes with some deviations, implying the presence of both surface-controlled capacitive and Faradaic redox reactions. The C-BCLP electrode shows excellent capacitive performance with a high specific capacitance value of 338.3 F g^{-1} at 1 A g^{-1}, which is significantly higher than that of the C-BCP electrode (294.2 F g^{-1} at 1 A g^{-1}) (Fig. 6b). To compare the specific capacitance value of the C-BCLP electrode, the specific capacitance value of the S-Carbon electrode obtained from the previous study using LS-impregnated BC was found to be 272.6 F g^{-1} at 1 A g^{-1}, whereas the undoped carbon electrode showed a specific capacitance value of only 215.3 F g^{-1} at the same current density[19]. The high electrochemical performance of the current system can be attributed to heteroatom co-doping with N and S, providing extra sites for reactions, coupled with Fe_3O_4 nanoparticles that enhance the electrical conductivity of the carbon matrix.

Moreover, the capacitance of the C-BCLP electrode is retained at 100 F g^{-1} at a high current density of 20 A g^{-1}, signifying the excellent rate capability of the electrode. On the contrary, the capacitance of the S-carbon electrode in the previous work decreased from 272.6 to 153.8 F g^{-1} with increasing current density from 1 to 10 A g^{-1}[19]. Though sulfur doping in the earlier work facilitated the accessibility of ions and the presence of pseudocapacitance effects, the capacitance of the newly synthesized material is better due to the presence of additional pathways for conductivity from the PPy-derived carbon matrix and the synergistic effects of the carbon and Fe_3O_4 nanoparticles. The smaller IR drop for the C-BCLP electrode is another indicator of the low internal resistance and high electrical conductivity of the electrode material.

To explore the charge transfer kinetics at the electrodes, EIS measurements were performed. From the Nyquist plots, it is found that the diameter of the semicircle in the high-frequency region is smaller for C-BCLP compared to C-BCP, which indicates that the charge transfer resistance (R_{ct}) is lower for C-BCLP

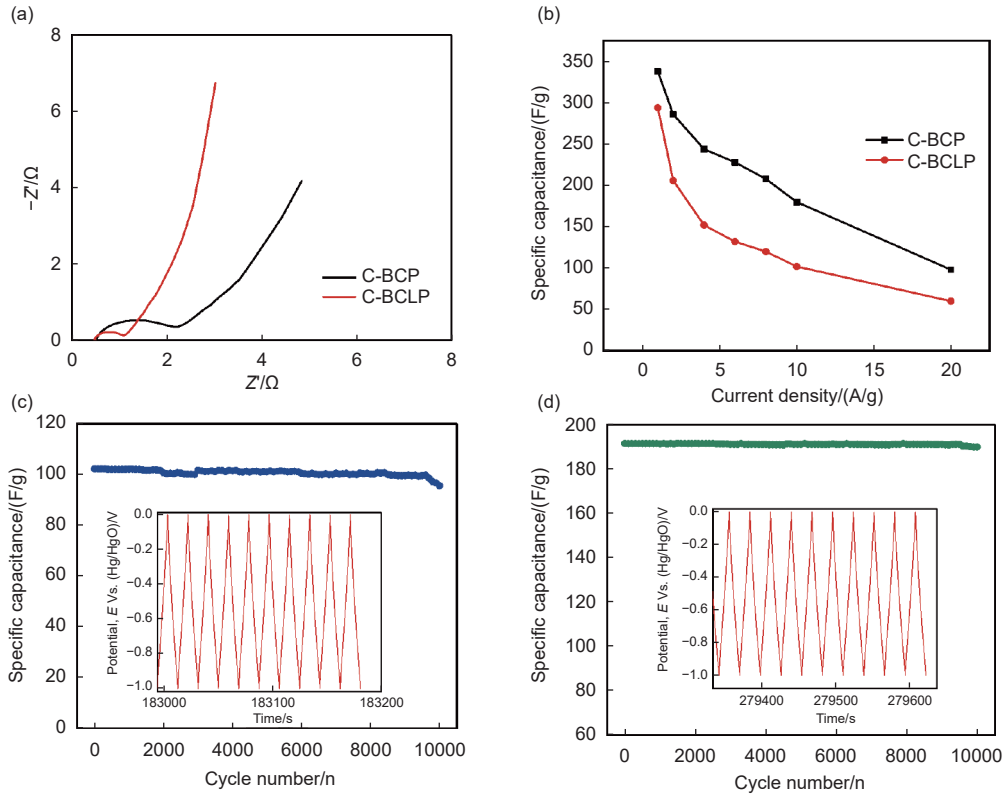

Fig. 6 Electrochemical performance of the C-BCP and C-BCLP electrodes in the electrolyte solution of 3 mol L^{-1} KOH: (a) Nyquist plots from EIS spectra, (b) specific capacitance vs. current density, and cycling stability curves of (c) C-BCP and (d) C-BCLP electrodes after 10 000 cycles at constant current density, and the corresponding GCD curves of the last few cycles are presented in the insets

(Fig. 6a). The values of R_s and R_{ct} for C-BCP are 0.27 and 1.12 Ω, respectively, whereas for C-BCLP, these values are lower at 0.23 and 0.55 Ω, respectively. In the case of our previously developed system, the R_s and R_{ct} values for the S-carbon electrode were 0.35 Ω and 1.45 Ω, respectively, which were much lower compared to the undoped carbon electrode (R_s = 0.39 Ω and R_{ct} = 2.58 Ω)[19]. Notably, in the present C-BCLP system, the charge transfer characteristics at the electrode/electrolyte interface have been enhanced as reflected by the higher slope in the low-frequency region of the Nyquist plot. This is because the Fe_3O_4 nanoparticles uniformly dispersed in the N/S co-doped carbon matrix can facilitate the efficient charge transportation and carbon-metal oxide coupling, thus enhancing the electrochemical kinetics of the electrode material.

Cycling stability tests prove the excellent stability of the C-BCLP electrode. The capacitance retention of the electrode is approximately 99% with 190.1 F g^{-1} after 10 000 cycles at 10 A g^{-1} (Fig. 6d), with excellent charge and discharge curves, whereas C-BCP shows 94% retention with specific capacitance 95.7 F g^{-1} at 10 A g^{-1} (Fig. 6c). By comparison, the S-carbon electrode in the previous work only retained 86% of capacitance after 5000 cycles at 6 A g^{-1}[19]. The comparative electrochemical study proves that the fabricated N-doped C/Fe_3O_4 and N,S-doped C/Fe_3O_4 show better supercapacitive performance than other Fe_3O_4 electrode materials reported to date. The N,S-doped C/Fe_3O_4 electrode material showed an outstanding specific capacitance of 338.3 F g^{-1} at 1 A g^{-1} along with outstanding cycle stability after 10 000 cycles with 190.1 A g^{-1} (99% retention capacity), surpassing most of the Fe_3O_4/carbon electrode materials available in literature (Table 1). The improved electrochemical performance is due to the cooperative effect of dual heteroatoms (N,S) doping and the carbon matrix, leading to increased electrical conductivity, more electroactive sites, and fast charge transfer reactions. Thus, the findings suggest that the fabricated N,S-doped C/Fe_3O_4 could be considered an ideal electrode material for supercapacitors. The excellent stability of the electrode in the present work can be ascribed to the excellent stability of the fibrous framework from bacterial cellulose and the role of the polymer-derived carbon matrix in immobilizing the Fe_3O_4 nanoparticles and preventing their aggregation during the charge and discharge processes.

Overall, these results clearly demonstrate the progressive improvement in electrochemical performance that is facilitated through rational precursor design. Whereas the incorporation of sulfur into the earlier synthesized BC-based carbon helped to optimize the interaction with the electrolyte as well as the pseudocapacitance, the PPy-incorporated LS-BC-based carbon/Fe_3O_4 composite further adds benefits such as electrical conductivity and structural stability. The hierarchical porosity, as well as the N/S doping, of the carbon structure results in the creation of many active centers that facilitate ion transport. This, coupled with the introduction of Fe_3O_4, helps to optimize the charge transfer processes within the electrode matrix.

Table 1 Comparison of the electrochemical performance parameters of previously studied Fe_3O_4/carbon composite electrode materials and the currently developed N-doped C/Fe_3O_4 and N,S-doped C/Fe_3O_4 electrodes for use in supercapacitors

Electrode material	Electrolyte	Voltage window/V	Specific capacity/(F g^{-1})	Cycle life (F/g)	Ref.
Fe_3O_4/C	1 M Na_2SO_4	−1.2 – 0	136 at 1 A g^{-1}	115 after 1000 cycles at 2 A g^{-1}	[32]
Fe_3O_4-C core-shell microspheres	1 M KOH	−1 – 0.5	110.8 at 0.5 A g^{-1}	71.2 after 1500 cycles at 1 A g^{-1}	[33]
Fe_3O_4-C PorousNanorods	2 M KOH	−0.8 – 0.2	285.4 at 1 A g^{-1}	220.5 after 5000 cycles at 2 A g^{-1}	[34]
C-coated Fe_3O_4	1 M Na_2SO_4	−1.0 – 0	150 at 1.5 A g^{-1}	—	[35]
Porous Fe_3O_4/carbon composite	1 M KOH	−1.0 -0	139 at 1 A g^{-1}	4000 cycles	[36]
C from BC	3 M KOH	−1.0 - 0	215.3 at 1 A g^{-1}	5000 cycles	[19]
S-doped carbon from BC	3 M KOH	−1.0 - 0	272.6 at 1 A g^{-1}	148.1 after 5000 cycles at 6 A g^{-1}	[19]
N-doped C/Fe_3O_4	3 M KOH	−1.0 - 0	294.2 at 1 A g^{-1}	95.7 after 10 000 cycles at 10 A g^{-1}	This work
N/S-doped C/Fe_3O_4	3 M KOH	−1.0 - 0	338.3 at 1 A g^{-1}	190.1 after 10 000 cycles at 10 A g^{-1}	This work

Note: M: mol L^{-1}

4 Conclusion

A heteroatom-doped carbon/Fe_3O_4 composite was synthesized through the carbonization of a bacterial cellulose-lignosulphonate-polypyrrole precursor in the presence of $FeCl_3$. Structural analysis confirmed the formation of a hierarchical porous carbon matrix with uniformly dispersed Fe_3O_4 nanoparticles. The presence of Fe_3O_4 was verified by XRD analysis, while SEM and TEM images showed the hierarchical porous structure of the composite. Elemental mapping and XPS analyses further confirmed the homogeneous distribution of C, O, N, S, and Fe elemennts, as well as the successful doping of N/S heteroatoms into the material. The presence of Fe^{2+} and Fe^{3+} was also confirmed. Due to the presence of both N/S doped carbon and Fe_3O_4 nanoparticles, the C-BCLP material showed a high specific capacitance of 338.3 F g^{-1} at 1 A g^{-1} and excellent electrochemical stability by retaining 99% of the initial specific capacitance even after 10 000 cycles at 10 A g^{-1}. The material also showed excellent rate performance. The above results clearly confirm the biomass-derived composite material as an electrode material for the fabrication of supercapacitors.

References

[1] Olabi AG, Abbas Q, Al Makky A, et al. Supercapacitors as next generation energy storage devices: Properties and applications[J]. Energy, 2022, 248: 123617.

[2] Pathak M, Bhatt D, Bhatt R C, et al. High energy density supercapacitors: an overview of efficient electrode materials, electrolytes, design, and fabrication[J]. The Chemical Record, 2024, 24(1): e202300236.

[3] Rani S, Kumar P, Tandon A, et al. Recent advancements in supercapacitor-integrated self-powered sensors[J]. Chemical Engineering Journal, 2026, 530: 173558.

[4] Alharbi A. Boosting supercapacitor performance through innovative transition metal-based electrode materials[J]. RSC advances, 2025, 15(41): 34551-34582.

[5] Davies A, Yu A. Material advancements in supercapacitors: from activated carbon to carbon nanotube and graphene[J]. The Canadian Journal of Chemical Engineering, 2011, 89(6): 1342-1357.

[6] Dubey R, Guruviah V. Review of carbon-based electrode materials for supercapacitor energy storage[J]. Ionics, 2019, 25(4): 1419-1445.

[7] Sharma G, Sharma S, Kumar A, et al. Activated carbon as superadsorbent and sustainable material for diverse applications[J]. Adsorption Science & Technology, 2022, 2022: 4184809.

[8] Sun L, Gong Y, Li D, et al. Biomass-derived porous carbon materials: synthesis, designing, and applications for supercapacitors[J]. Green Chemistry, 2022, 24(10): 3864-3894.

[9] Yin Y, Liu Q, Zhao Y, et al. Recent progress and future directions of biomass-derived hierarchical porous carbon: Designing, preparation, and supercapacitor applications[J]. Energy & Fuels, 2023, 37(5): 3523-3554.

[10] Ma L, Bi Z, Xue Y, et al. Bacterial cellulose: an encouraging eco-friendly nano-candidate for energy storage and energy conversion[J]. Journal of Materials Chemistry A, 2020, 8(12): 5812-5842.

[11] Wu Z, Chen S, Li J, et al. Insights into hierarchical structure–property–application relationships of advanced bacterial cellulose materials[J]. Advanced Functional Materials, 2023, 33(12): 2214327.

[12] Bai Q, Xiong Q, Li C, et al. Hierarchical porous carbon materials from poly (methyl methacrylate)/bacterial cellulose composite monolith for high-performance supercapacitor electrodes[J]. ACS Sustainable Chemistry & Engineering, 2017, 5(10): 9390-9401.

[13] Bai Q, Xiong Q, Li C, et al. Hierarchical porous carbon materials from a sodium alginate/bacterial cellulose composite for high-performance supercapacitor electrodes[J]. Applied Surface Science, 2018, 455: 795-807.

[14] Lei W, Jin D, Liu H, et al. An overview of bacterial cellulose in flexible electrochemical energy storage[J]. ChemSusChem, 2020, 13(15): 3731-3753.

[15] Chashiro K, Iwasaki S, Hasegawa T, et al. Integrating polyacrylonitrile (PAN) nanoparticles with porous bacterial cellulose hydrogel to produce activated carbon electrodes for electric double-layer capacitors[J]. Microporous and Mesoporous Materials, 2021, 323: 111209.

[16] Li E, Liu R, Huang S, et al. Flexible N-doped active carbon/bacterial cellulose paper for supercapacitor electrode with high areal performance[J]. Synthetic Metals, 2017, 226: 104-112.

[17] Zhang K, Irmak S, Catchmark J M. Preparation and properties of heteroatom-doped bacterial cellulose-derived carbonaceous materials[J]. Carbohydrate Polymer Technologies and Applications, 2023, 6: 100400.

[18] Liu W, Peng D, Liu X, et al. Defect-engineered sulfur-doped carbon nanofibers derived from bacterial cellulose for high-rate sodium-ion storage[J]. Journal of Energy Storage, 2026, 141: 119484.

[19] Rao K M, Prasad M S, Rosaiah P, et al. Sustainable supercapacitors of sulfur-doped carbon from environmentally friendly sodium lignosulfonate impregnated with bacterial cellulose[J]. International Journal of Biological Macromolecules, 2024, 282: 137067.

[20] Zhang G, Liu X, Wang L, et al. Recent advances of biomass derived carbon-based materials for efficient electrochemical energy devices[J]. Journal of Materials Chemistry A, 2022, 10(17): 9277-9307.

[21] Zhu J, Xu Y, Zhang Y, et al. Porous and high electronic conductivity nitrogen-doped nano-sheet carbon derived from polypyrrole for high-power supercapacitors[J]. Carbon, 2016, 107: 638-645.

[22] Wang T, Wang L X, Wu D L, et al. Interaction between nitrogen and sulfur in co-doped graphene and synergetic effect in supercapacitor[J]. Scientific reports, 2015, 5(1): 9591.

[23] Zhi M, Xiang C, Li J, et al. Nanostructured carbon–metal oxide composite electrodes for supercapacitors: a review[J]. Nanoscale, 2013, 5(1): 72-88.

[24] Tipsawat P, Wongpratat U, Phumying S, et al. Magnetite (Fe_3O_4) nanoparticles: Synthesis, characterization and electrochemical properties[J]. Applied Surface Science, 2018, 446: 287-292.

[25] Sinan N, Unur E. Fe_3O_4/carbon nanocomposite: Investigation of capacitive & magnetic properties for supercapacitor applications[J]. Materials Chemistry and Physics, 2016, 183: 571-579.

[26] Lakshmi C, Balraju P, Muthukumarasamy N, et al. Investigation of co-doped magnetite (Fe_3O_4) nanomaterials with reduced graphene oxide and bismuth for photocatalytic, supercapacitor, and antimicrobial applications[J]. Electrochimica Acta, 2025, 511: 145376.

[27] Karakoç T. Structural design of inorganic transition metal oxide/carbon composite materials for optimizing their electrochemical performance in energy storage devices [D]. Université de Strasbourg, 2024.

[28] Chitte H K, Shinde G N, Bhat N V, et al. Synthesis of polypyrrole using ferric chloride ($FeCl_3$) as oxidant together with some dopants for use in gas sensors[J]. Journal of sensor technology, 2011, 1(2): 47.

[29] Li Q, Zhang Y, Song Y, et al. Apple residues derived porous carbon nanosheets synthesized with $FeCl_3$ assisted hydrothermal carbonization for supercapacitors with high rate performance[J]. Carbon Letters, 2023, 33(2): 549-560.

[30] Kang J, Hu C, Liu X, et al. One-pot synthesis of magnetic nanocellulose/Fe_3O_4 hybrids using $FeCl_3$ as cellulose hydrolytic medium and Fe_3O_4 precursor[J]. ACS Sustainable Chemistry & Engineering, 2024, 12(15): 5917-5926.

[31] Zhang L L, Gu Y, Zhao X S. Advanced porous carbon electrodes for electrochemical capacitors[J]. Journal of Materials Chemistry A, 2013, 1(33): 9395-9408.

[32] Hani N A, Faisal S A, Walid M. D. Magnetic iron oxide (Fe_3O_4)/carbon nanostructures as cost-effective bifunctional electrodes for energy storage (supercapacitors) and water splitting (OER)[J]. RSC Advances, 2026, 16(29): 26880-26895.

[33] Pu J, Shen L, Zhu S, et al. Fe_3O_4@C core–shell microspheres: synthesis, characterization, and application as supercapacitor electrodes[J]. Journal of Solid State Electrochemistry, 2014, 18(4): 1067-1076.

[34] Wang L, Yu J, Dong X, et al. Three-dimensional macroporous carbon/Fe_3O_4-doped porous carbon nanorods for high-performance supercapacitor[J]. ACS Sustainable Chemistry & Engineering, 2016, 4(3): 1531-1537.

[35] Kumar R, Nekouei RK, Sahajwalla V. In-situ carbon-coated iron oxide (ISCC-Fe_3O_4) as an efficient electrode material for supercapacitor applications[J]. Ceramics International, 2025, 51(9): 12312-12320.

[36] Meng W, Chen W, Zhao L, et al. Porous Fe_3O_4/carbon composite electrode material prepared from metal-organic framework template and effect of temperature on its capacitance[J]. Nano Energy, 2014, 8: 133-140.